

## DEFORMABLE RF FINGERS WITH AXIAL EXTENSION

S. Sharma<sup>†</sup>, F. DePaola, F. Lincoln, J. Tuozzolo, NSLS-II, BNL, 11973 Upton, NY, USA

### Abstract

RF fingers in a bellows assembly provide electrical continuity for the image current between adjacent vacuum chambers. They are required to absorb all misalignments between the two chambers while minimizing abrupt changes in the beam aperture. In addition, during bake-outs of the chambers the fingers are required to accommodate their large thermal expansions. The latter is achieved either by having a sliding-contact finger design or a deformable finger design. In this paper we describe a version of the deformable finger design which permits large compression, significant misalignments and axial extension. A novel method of fingers' fabrication, FE analysis and test results are presented.

### INTRODUCTION

Bellows assemblies are used as flexible interconnections between adjacent vacuum chambers. The flexibility of the stainless steel bellows compensates for transverse misalignments and axial gap of  $\sim 2$  mm for the NSLS-II chambers. During bake-outs of the vacuum chambers the bellows compress by  $\sim 10$  mm to absorb the combined thermal expansion of the chambers. RF fingers made from copper alloys are used inside the bellows to provide electrical continuity and the continuity of the beam aperture. These fingers must also compensate for the chambers' misalignment, axial gap and thermal expansion.

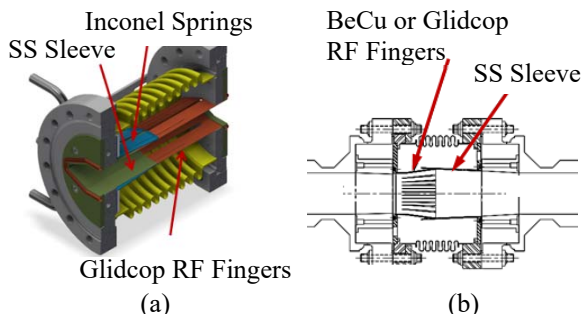


Figure 1: Conventional designs of RF fingers sliding on SS sleeve, (a) outside sliding type, (b) inside sliding type.

The conventional design of RF fingers relies on the fingers sliding on the outside surface or on the inside surface of a sleeve usually made from stainless steel. RF fingers for NSLS-II [1] and APS [2], shown in Fig. 1(a) and 1(b), are examples of the two designs. In the case of the outer-sliding RF finger design the fingers are compressed by cantilevered Inconel springs to ensure good contact pressure. A lack of good contact pressure can lead to thermal deformation and even melting of the fingers in storage rings with high beam current or high current per bunch.

<sup>†</sup> sharma@bnl.gov

A deformable finger design with fixed contacts has been proposed recently [3, 4] for the interconnection module of the LHC vacuum chambers. The RF fingers are pre-deformed in a corrugated shaped (Fig. 2(a)). The design is optimized to prevent buckling and over-extension. In the as-installed position, Fig. 2 (a), the fingers are compressed. During operation the fingers are almost fully extended (Fig. 2(b)) leaving some slack to compensate for axial gap.



Figure 2: LHC deformable finger design, (a) as installed, (b) in operation.

In this paper we present a fixed-contact RF finger design that utilizes large nonlinear deformation including buckling to compensate for thermal expansion of the chambers. The RF fingers in this single-piece design can be offset by up to 2 mm to compensate for transverse misalignments between the vacuum chambers. They can also be extended by up to 2 mm to compensate for axial gaps. The RF fingers are designed to remain straight during operation.

### PROPOSED DESIGN

Figure 3 depicts the proposed design of the RF fingers with typical overall dimensions. RF fingers are made as a single-piece spool (Fig. 3(a)) from a stock of CuCrZr or Glidcop (AL-15) alloys. These alloys are chosen in place of a more commonly used alloy, BeCu, because of their higher electrical and thermal conductivities (Table 1). Glidcop RF fingers are in use at PEP-II [5], APS and NSLS-II, and CuCrZr RF fingers have been proposed for the ITER project [6].

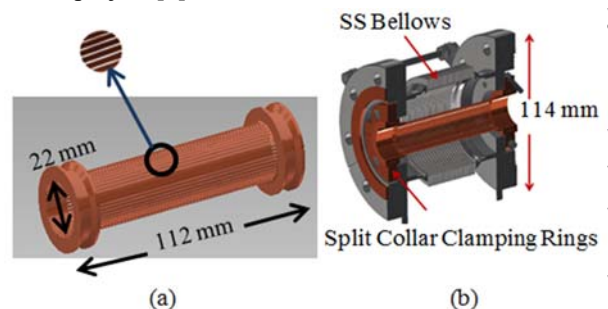


Figure 3: Proposed RF finger design, (a) single-pièce RF finger spool, (b) assembly inside SS bellows using split collar clamping rings.

Table 1: Electrical and Thermal Conductivities

Conductivity	Glidcop (AL-15)	CuCrZr C18150	BeCu C172000
Thermal (W/m.K)	365	320	107
Electrical (%IACS)	92	76-90	22

During installation the RF fingers can be extended by up to 2 mm to compensate for axial gap. Therefore, the temper for Glidcop or CuCrZr is selected for higher elongation at fracture (preferably > 15%) instead of higher ultimate strength. The elongation at fracture can vary from 6% to 30% depending on the shapes (thin sheets to round bars) and temper [7, 8].

The RF-finger spool is integrated in the bellows assembly by split-collar clamping rings (Fig. 3(b)) which can be joined tightly for good electrical and thermal contacts. The two ends of a CuCrZr RF-finger spool can also be directly welded to stainless steel flanges using a process developed at TPS [9].

The design of the RF finger spool and its manufacturing is illustrated in Fig. 4. A hollow pipe of 112 mm length with two grooved ends is first created by machining (drilling and turning in this example). The inside bore of the pipe,  $\phi$  19 mm, is machined to be 3 mm smaller than the required beam aperture ( $\phi$  22 mm) for rigidity. The outer profile in the center is made 3.4 mm thicker than the bore providing RF fingers of 0.4 mm thickness. A wire electric-discharge machining (EDM) is used to remove the extra 3 mm thickness of the inside profile. In the same EDM setup the cutting wire is moved in and out radially by 0.4 mm beyond the inside profile, repeating it every  $7.2^\circ$  circumferentially. This leads to 50 fingers of approximately 1.25 mm width at the beam aperture profile. A distinct advantage of this manufacturing approach is that the RF-fingers' profile can be matched to the beam aperture profile of any geometry (e.g., elliptical) without any step discontinuity.

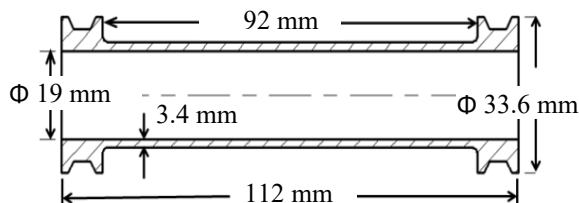


Figure 4 : RF-finger spool before wire EDM cut. EDM enlarges the inside profile by 3 mm and creates 50 fingers of 0.4 mm thickness by radial cuts at  $7.2^\circ$ .

During the bellows assembly process an axial compression of 10 mm is applied to the RF-finger spool. The fingers are guided to bend radially outward by a small inflatable rubber tube placed inside the bore. Residual stresses developed from this initial preset ensure that in subsequent cycles the fingers would bend outward.

## FINITE ELEMENT ANALYSIS

An ANSYS finite element analysis was performed for a single flat finger of 72 mm length, 1.25 mm width and 0.4 mm thickness. As shown in Fig. 5, two stiffened ends of 10-mm length were added to represent the ends of the RF finger spool and to apply fixed and displacement boundary conditions (BCs). One of the ends was fixed in all three directions whereas displacement BC was applied to the other end to simulate transverse tolerances, axial gap and compression during bakeout. The analysis included large deformation with stress stiffening and a bilinear elastic-plastic material model with kinematic hardening. An elastic modulus of 125 GPa, yield stress of 350 MPa, Poisson's ratio of 0.3 and tangent modulus of 1,300 MPa were specified based on mechanical properties of CuCrZr at room temperature.

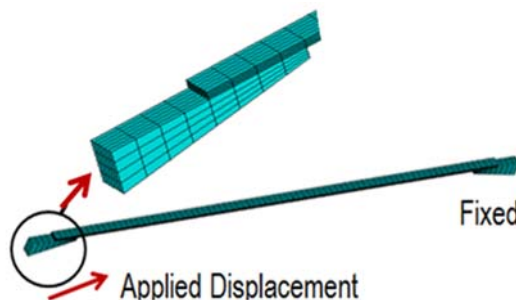


Figure 5: Finite element model of a single RF finger. Displacement BCs are applied to one end representing transverse offset (3mm), axial gap (3mm) and displacement cycles in the range +3 mm to -12 mm.

The analysis was performed for 3 compression cycles. In the first cycle a compressive displacement of 6 mm is applied to introduce preset in the fingers. In the preset cycle itself the buckling direction is imposed by an artificial pressure of 0.03 MPa during the initial 1 mm of compression. The transverse offset of 3 mm and the axial extension of 3 mm are applied after the preset cycle. The applied axial displacement is then changed from +3 mm to -12 mm in the next 2 cycle to simulate compression during bake-outs.

Figure 6 shows transverse deflection of the finger at the center ( $U_y$ ) versus axial displacement ( $D_x$ ). Data from an experimental test (described in the next section) for the compression part of the first compression cycle is also plotted showing a good match between the ANSYS and test results. The two curves for the compression cycles are essentially the same. The results show that  $U_y$  is several times ( $\sim 5$ ) larger than  $D_x$  at the beginning of compression but by the end of compression  $U_y = 0.6 D_x$ . A maximum  $U_y$  of 20.6 mm is obtained at full compression,  $D_x = -12$  mm.

Content from this work may be used under the terms of the CC BY 3.0 licence (© 2018). Any distribution of this work must maintain attribution to the author(s), title of the work, publisher, and DOI.

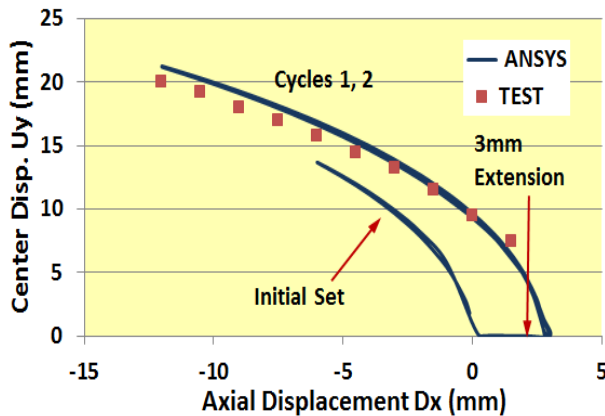


Figure 6: Transverse displacement at the center,  $U_y$ , versus applied axial displacement,  $D_x$ , for the initial preset cycle, 3 mm extension and 2 compression cycles.

Equivalent stress contours at the end of the first compression cycle are shown in Fig. 7. The equivalent stress is maximum (437 MPa) at the center and is considerable above the yield stress of 350 MPa, which is indicative of large plastic deformation.

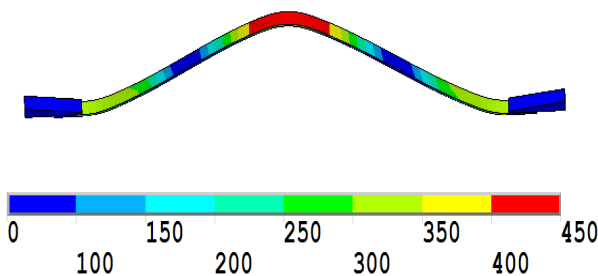


Figure 7: Equivalent stress (MPa) contours at the end of the first compression cycle.

Axial stress and strain at the center (top) are plotted in Fig. 8 starting from 3 mm extension to the end of the first compression cycle. The preset cycle and the second compression cycle are omitted for clarity. In the figure, letters A to F denote the following load excursions: A: 3 mm extension to the nominal position denoted by ●, B+C buckling at the beginning of compression cycle, D: continued compression, E: extension and F: stress reversal in extension.

Large tensile plastic deformations occur during the 3 mm extension, A, and continued compression beyond buckling. During extension, E, there is elastic unloading followed by a large compressive plastic deformation and then by a tensile reversal which straightens the finger. Axial strain at the nominal position is ~ 4% and the strain range for the compression-extension cycle is 3.3%. In the second compression cycle (not shown) the strain range reduces to 2.69% due to mean stress-strain relaxation.

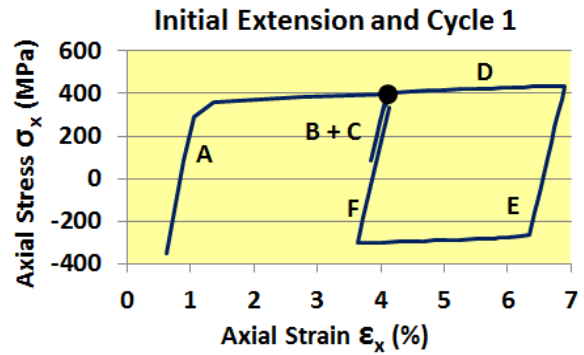


Figure 8: Axial stress versus axial strain at the center-top of the finger for 3 mm extension and the first compression-extension cycle. A: 3 mm extension, B+C: buckling at the start of compression, D: continued compression, E: extension and F: stress reversal in extension.

## EXPERIMENTAL TESTS

Experimental tests were performed to determine the low-cycle fatigue life of the RF fingers. Initially the RF fingers were made in a planar geometry for ease of fabrication and testing. Subsequently the tests were repeated on RF finger spools of the geometry shown in Fig. 4.

### Planer RF Fingers

The Planer RF fingers were made from 50 mm-thick plates of CuCrZr and Glidcop. Thin plates, of 106 mm x 60 mm size, were first made by wire EDM. The cross-section of the thin plates had a thickness 3 mm larger in the middle than the cross section shown in Fig. 9(a). In the second wire EDM step the extra 3 mm thickness was removed and 0.4 mm deep cuts were made for the fingers (Fig. 9(b)). The test samples of 3 fingers each (Fig. 9(c)) were then cut from the larger sample.

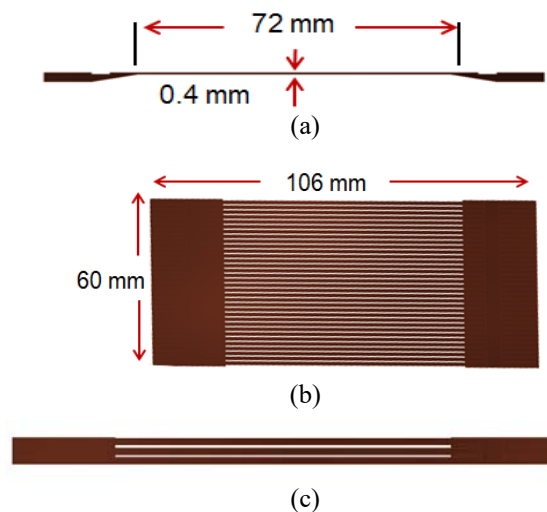


Figure 9: Wire EDM of the RF fingers, (a) cross section of the fingers, (b) fingers in the thin plate, (c) test sample of 3 fingers.

Content from this work may be used under the terms of the CC BY 3.0 licence (© 2018). Any distribution of this work must maintain attribution to the author(s), title of the work, publisher, and DOI.

The test setup for cyclic fatigue testing of the fingers is shown in Fig. 10. Clamping fixtures holding the two ends of the fingers were attached to the two jaws of a precision machine vise. One of the clamping fixtures was adjustable and provided a transverse offset of 2-3 mm. The vise was operated manually to apply compression cycles. A Starrett® dial indicator (0.025 mm resolution) was placed between the jaws to measure the applied displacement. Another dial indicator (not shown) was used for one compression cycle to measure the transverse displacement at the center of the finger.



Figure 10: Test setup for cyclic fatigue testing of the RF fingers.

Four test samples, 2 of CuCrZr and 2 of Glidcop were cycled to fatigue failure. All samples had an initial preset compression cycle of 6 mm, a transverse offset of 3 mm and an axial extension of 3 mm. The first CuCrZr and Glidcop samples were guided to buckle upward by a slight application of index-finger pressure. The second CuCrZr and Glidcop samples were guided to buckle downward which is opposite to the direction preferred by the finger geometry.

Table 2 shows number of compression cycles to failure for the 4 test samples with 3 fingers each. Bending in the reverse direction reduced the cycles to failure significantly. In all cases the cycles to failure exceeded the expected number (< 30) of bake-outs of the chambers during the life time of the machine. Glidcop fingers showed a better fatigue life than the CuCrZr fingers. Subsequent tensile tests showed that elongations to failure for the CuCrZr and Glidcop fingers were 7.6% and 11.6%, respectively. A higher elongation to failure, >15%, can be specified with the selection of proper shape and temper of the copper-alloy stock.

Table 2: Compression Cycles to Fatigue Failure

Test Sample	CuCrZr		Glidcop	
	1	2	1	2
Finger 1	130	69	268	208
Finger 2	199	74	288	218
Finger 3	222	158	392	225

Deformed shapes of the fingers for different cycles were almost identical up to a few cycles (~ 10) before failure. In the last few cycles the fingers start separating with kinks appeared at the center. The fingers broke in the

middle except for a couple of cases when they broke at the ends. For the Glidcop sample 1, the normal bent shape (cycle 200) is shown in Fig. 11(a), extended shape at the second finger break (cycle 288) in Fig. 11(b), and the shape at the third finger break (392 cycles) in Fig. 11(c).

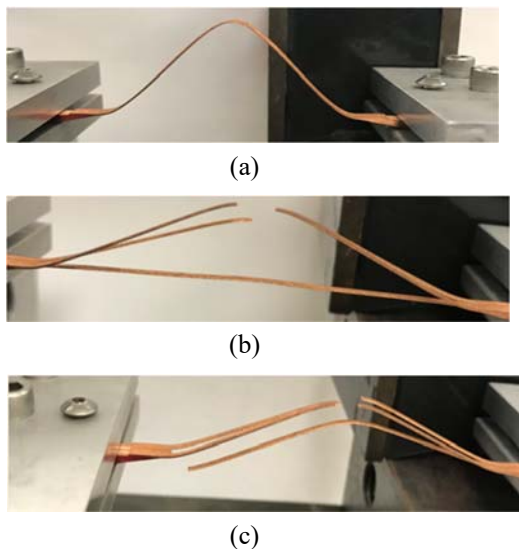


Figure 11: Deformed shapes of the fingers of Glidcop sample 1: (a) nominal bent shape after 200 cycles, (b) extended shape at the second finger break after 288 cycles, (c) shape at the third finger break after 392 cycles.

### RF Finger Spools

RF finger spools were tested with the same test setup as described above but with different clamping fixtures. Three spools were tested, one made from CuCrZr and the other two made from Glidcop AL-15. The CuCrZr spool and the first Glidcop spool had 10 mm taper at the top ends of the fingers (see Fig. 12(a)) instead of a 1 mm radius (Fig. 12(b)) used for the second Glidcop spool. Eliminating the taper increased the effective length of the fingers from 72 mm to 90 mm (see Fig. 4).

The CuCrZr spool and its setup experienced two problems. A preset compression of 12 mm (compared to 6 mm for the planer fingers) was applied to ensure that higher residual stresses will result in outward bending in the subsequent compression cycles. The higher compression, however, kinked the fingers in the middle. The aluminium clamping fixtures also turned out to be weak. They distorted when a 2 mm extension was applied causing uneven extension and probably a reduction in fatigue life. Thicker steel clamping fixtures were used for the Glidcop spools and only 10 mm of preset compression was applied. For all three spools a small inflatable tube was used to control the bending direction during the preset compression cycle.

Before compression cycles a 2 mm transverse offset and a 2 mm extension was applied to the spools. Then the spools were cycled at different compression levels. The goal was not only to determine if the fingers could sur-

vive > 30 cycles at 10 mm compression, but also to see if cycles at higher compression levels were possible.

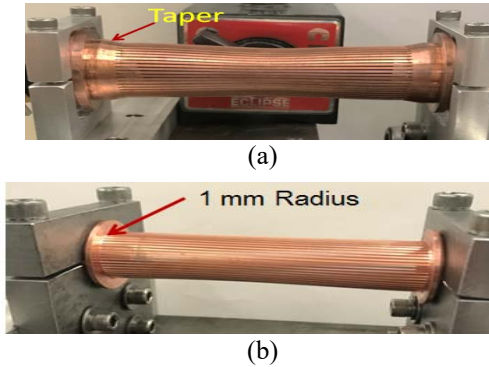


Figure 12: Test setup for the RF finger spools, (a) CuCrZr spool with aluminium clamping fixtures, (b) Glidcop spool with steel clamping fixtures.

There was no noticeable difference in the deformed shapes of the finger spools (see Fig. 13) during most of the cycles. The 10 mm tapers at the ends of the CuCrZr spool and Glidcop #1 spool appeared to keep the deformation symmetric even under the transverse offset of 2 mm. A few cycles before the break of a finger a small kink was usually formed at the failure location.

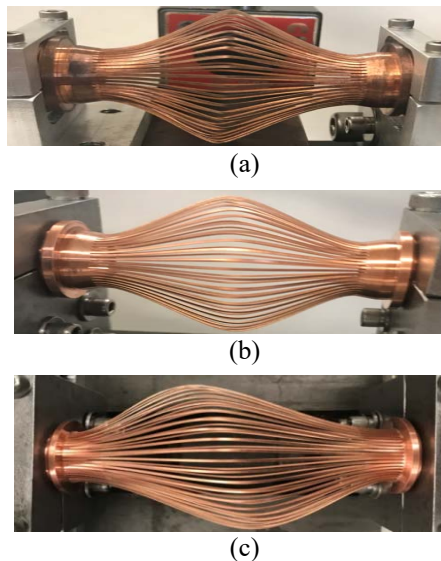


Figure 13: Deformed shapes of the finger spools during cyclic tests at 10 mm compression, (a) CuCrZr spool, (b) Glidcop spool #1, (c) Glidcop spool #2.

The results of cyclic tests are shown in Table 3. Following 30 cycles at 10 mm compression, the first break of a finger of CuCrZr spool occurred after only 8 additional cycles at 12 mm compression. The first finger of Glidcop spool # 1 (70 mm finger length) broke after 132 cycles at 10 mm compression. For Glidcop spool # 2 the first break occurred after a combined number of 137 cycles at different compression levels as follows: 50 cycles at 10 mm, 60 cycles at 12 mm and 27 cycles at 14 mm. The failure of the first finger occurred in the middle for the CuCrZr spool but at one of the ends for the Glidcop spools.

Table 3: Cyclic Tests on the RF Finger Spools – Number of Cycles at First Finger Break

CuCrZr Spool		Glidcop Spool # 1		Glidcop Spool # 2	
Compr. (mm)	Cycles	Compr. (mm)	Cycles	Compr. (mm)	Cycles
10	30	10	132	10	50
12	8			12	60
				14	27

## CONCLUSION

A new design of deformable RF fingers with fixed ends and axial extension is presented together with FE analysis and test results. Beam aperture through the RF fingers is continuous without steps. The design is based on large nonlinear deformation including buckling of the RF fingers. The RF finger spool piece is made from high conductivity copper alloys such as CuCrZr and Glidcop. Fabrication of the fingers requires simple machining (drilling, turning and EDM) operations. Cyclic fatigue tests on the RF finger spools show that the typical design requirements of transverse misalignment and axial gap can be met with a good safety margin. The margin is expected to increase further with the selection of a copper-alloy stock and its temper such that the minimum elongation to failure is > 15%.

## ACKNOWLEDGMENTS

The authors acknowledge the contributions of our co-workers M. Calderaro, A. DiMauro, J. Mondi, K. Wilson and the support of our Division Director, T. Shaftan.

## REFERENCES

- [1] C. Hetzel *et al.*, "Design and Fabrication of NSLS-II Storage Ring Vacuum Chambers and Components", in *Proc. IPAC2012*, New Orleans, Louisiana, USA, January 2012, paper WEPPD026, p2560.
- [2] J. Jones *et al.*, "APS SR Flexible Bellows Shield Performance", in *Proc. PAC99*, New York, USA, 1999, p3095.
- [3] C. Garion, *et al.*, "Development of a New RF Finger Concept for Vacuum Beamline Interconnections", in *Proc. IPAC2012*, New Orleans, Louisiana, USA, January 2012, paper WEPPD017, p2533.
- [4] C. Garion, "Design and Tests of the Shielded Beam Screen", HL-LHC Annual Meeting, Spain (2017). <https://indico.cern.ch/event/647714/timetable/?view=standard>.
- [5] M. Nordby *et al.*, "Bellows Design for PEP-II High Energy Ring Arc Chambers", in *Proc. PAC95*, Dallas, Texas, USA, 1995, p2048.
- [6] Arxiv, <https://arxiv.org/ftp/arxiv/papers/1710/1710.03632.pdf>.
- [7] <http://conductivity-app.org/alloy-sheet/19>.
- [8] <https://www.hoganas.com/en/business-areas/glidcop/>.
- [9] C-C. Chang, "Recent Vacuum R&D in Vacuum Group of TPS" (2017), [https://medsi.lbl.gov/NSLS\\_II\\_Seminar\\_Series\\_Talks-164.html](https://medsi.lbl.gov/NSLS_II_Seminar_Series_Talks-164.html)